Solar Water Splitting

DOI: 10.1002/ange.201305350

A Co-catalyst-Loaded Ta_3N_5 Photoanode with a High Solar Photocurrent for Water Splitting upon Facile Removal of the Surface Layer**

Mingxue Li, Wenjun Luo, Dapeng Cao, Xin Zhao, Zhaosheng Li, Tao Yu, and Zhigang Zou**

The consumption of fossil fuels creates energy shortage and serious environmental issues, which limit the sustainable development of the society. Solar energy is the most abundant renewable energy in the world. However, solar energy needs to be stored as chemical energy because of its low energy density, uneven distribution, and discontinuous radiation. Hydrogen is considered as a promising clean energy carrier for the future.[1] Solar water splitting produces hydrogen and oxygen, meanwhile, hydrogen can recombine with oxygen to produce water in a fuel cell and release the stored chemical energy to electricity. This energy cycle will be an ideal zero-carbon emission process. Since Fujishima and Honda originally reported that a TiO_2-based photoelectrochemical cell could be used to split water into hydrogen and oxygen in 1972,[2] intensive research has been done to improve the performance of the photoelectrochemical cell in the past forty years. However, the solar energy conversion efficiency is still low because of the intrinsic wide band gap of TiO_2.[3] It is necessary to explore some materials with narrower band gaps for high conversion efficiency.

In theory, a bias of 1.23 V is needed to split water into hydrogen and oxygen. If overpotential and resistance loss (about 0.6 V) are taken into account, a band gap with at least 1.8 eV will be necessary for a single material to split water, which does not match the optimum band gap (1.2–1.4 eV) for solar energy use by the Shockley-Queisser limit.[4] A p-n photoelectrochemical cell is a highly desirable approach to overcome the limit by two-photon absorption.[5,6] In this cell, a n-type photoanode (for water oxidation) is directly connected to a p-type photocathode (for proton reduction). Thus, a higher photovoltage can be obtained by assembling the two narrow-band-gap materials. On the other hand, photocurrent in a p-n photoelectrochemical cell is determined by the photoelectrode with the lower photocurrent. To date, several p-type semiconductor photocathodes with high solar photocurrent (dozens of $mA\,cm^{-2}$) have been developed.[7–10] Some promising visible-light-responsive photoanode materials, such as WO_3,[11,12] $BiVO_4$,[13–15] Fe_2O_3,[16,17] and Ta_3N_5,[18–24] have also been studied by us and other researchers. Though different methods, including ions doping,[13,17] morphology control,[11,24] heterojunction,[8,9,12,25] and particle necking[19,26] have been used to improve the performance of a photoanode, all of these photoanodes exhibit a much lower solar photocurrent (lower than $4\,mA\,cm^{-2}$)[12,13,16,24] than the photocathodes, which is a bottleneck for water splitting in a p-n photoelectrochemical cell. Therefore, finding an efficient photoanode is a key step in solar water splitting for hydrogen production.

Ta_3N_5 has a suitable band gap (2.1 eV) and band position, which is considered as a promising photoanode for solar water splitting without a bias. Thermal oxidation and nitridation of a Ta foil is a very convenient and reproduceable method for preparation of Ta_3N_5,[18,21] but the Ta_3N_5 photoelectrodes produced by this method indicated much lower performance than those of the samples prepared by other methods.[19,20,24] In this study, we prepared the Ta_3N_5 photoelectrodes by a modified thermal oxidation and nitridation method and found that the low efficiency of the Ta_3N_5 photoanode mainly from serious recombination of photogenerated carriers in the surface passivation layer of the sample. We obtained a high solar photocurrent of $5.5\,mA\,cm^{-2}$ at 1.23 V versus the reference hydrogen electrode (RHE) on the Ta_3N_5 photoanode by facile thermal or mechanical exfoliation of the surface recombination centers. To the best of our knowledge, this solar photocurrent is the highest value among all currently available Ta_3N_5 photoanodes.

The Ta foils were oxidized at different temperatures (550–610 °C) in air and then were nitrided at 850 °C in NH_3 flow (Figure S1). Interestingly, we observed that a thin surface layer was exfoliated from the sample when the Ta foil was oxidized at 590 or 610 °C and then nitrided. However, no such surface exfoliation happened when the Ta foils were oxidized at lower temperatures (550 and 570 °C) and then nitrided. To understand the surface thermal exfoliation process more clearly, SEM was used to investigate the changes in the morphologies of the samples prepared at different oxidation temperatures. The surface of the Ta_3N_5 sample at 550 (Figure 1a) and 570 °C (Figure 1b) are smooth and compact,

[*] M. Li,[+] Dr. W. Luo,[+] X. Zhao, Prof. T. Yu, Prof. Z. Zou
Ecomaterials and Renewable Energy Research Center
National Laboratory of Solid State Microstructures
Department of Physics, Nanjing University
Nanjing 210093 (P. R. China)
E-mail: wjluo@nju.edu.cn
zgzou@nju.edu.cn
D. Cao, Prof. Z. Li
College of Engineering and Applied Science
Nanjing University, Nanjing 210093 (P. R. China)

[+] These authors contributed equally to this work.

[**] This work is supported by the National Basic Research Program of China (973 Program, 2013CB632404) and the National Natural Science Foundation of China (No. 50902068, 51272101, 11174129). M. Li. is also supported by the Science Research Foundation of Graduate School of Nanjing University. We thank Mr. Robert Rozansky of Brown University for his editing of English.

Supporting information for this article is available on the WWW under http://dx.doi.org/10.1002/anie.201305350.

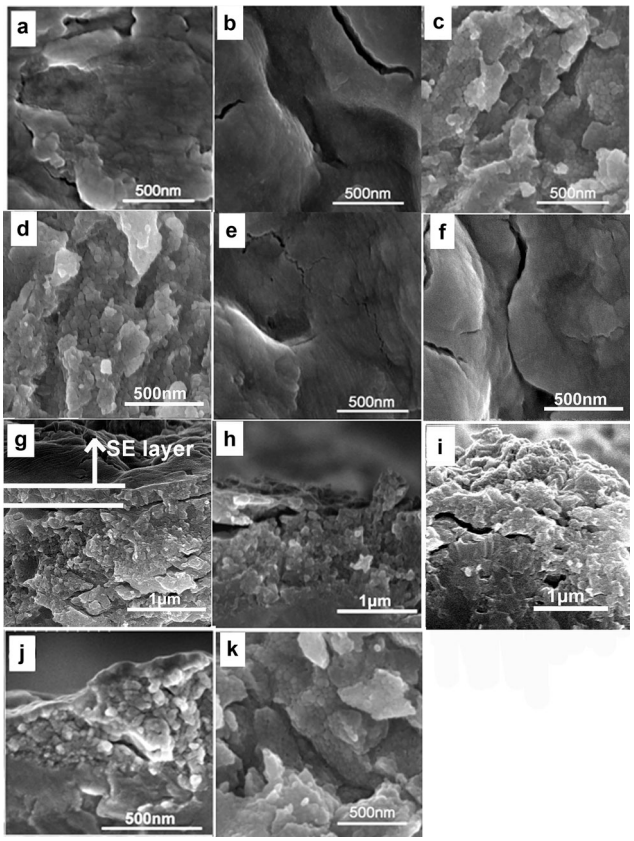

Figure 1. SEM images of the Ta_3N_5/Ta electrodes at different oxidation temperatures. The surface of Ta_3N_5 at a) 550 °C, b) 570 °C, c) 590 °C, and d) 610 °C. The surface of the exfoliated layer from Ta_3N_5 at e) 590 °C and f) 610 °C. The cross-section of Ta_3N_5 at g) 570 °C (SE layer = surface exfoliation layer), h) 590 °C, i) 610 °C, and j) 550 °C. k) The surface of Ta_3N_5 at 570 °C after mechanical surface exfoliation with scotch tape.

similar to the results in the previous study.[18,21] For the Ta_3N_5 samples at 590 and 610 °C, a thin layer was exfoliated from the surface after nitridation and a rougher surface with aggregated Ta_3N_5 particles was observed (Figure 1 c, Figure 1 d). However, the surface morphology of the exfoliation layer (Figure 1 e, Figure 1 f) is exactly similar to the surface morphologies of the samples at 550 and 570 °C. To further investigate the reasons for surface thermal exfoliation (the oxidation temperature or the thickness of the Ta_2O_5 film), we also prepared Ta_2O_5 at 550 °C for a longer time (1 hour) and at 610 °C for a shorter time (5 minutes), and then nitrided Ta_2O_5 to yield Ta_3N_5. We observed the surface exfoliation from the sample at 550 °C for 1 hour, whereas no surface exfoliation from the sample was observed at 610 °C for 5 minutes. Therefore, the surface thermal exfoliation depends on the thickness of the Ta_2O_5 film, not the oxidation temperature. We found that the critical thickness of Ta_2O_5 was about 2.5 μm (Figure S2) for surface exfoliation. When the Ta_2O_5 film is thicker than the critical thickness, the surface layer will be exfoliated after nitridation. A possible reason for the exfoliation is analyzed as follows. The densities of Ta_2O_5 and Ta_3N_5 are 8.2 $g\,cm^{-3}$ and 9.85 $g\,cm^{-3}$, respectively.[21] When Ta_2O_5 is nitrided into Ta_3N_5, the volume shrinks, which leads to an increase of stress in the Ta_3N_5 layer. In addition, the thicker the film, the larger is the stress.[27] When the Ta_2O_5 film is thicker than the critical thickness, the surface layer will be exfoliated during the transformation from Ta_2O_5 to Ta_3N_5 since some large cracks form to release the high stress in the film (Figure 1 g, 1 h, and 1 i). In previous studies, the Ta foils were only oxidized at 550 °C for a shorter time ($\leq$ 30 minutes),[18,21] the thickness of the Ta_2O_5 film was less than the critical thickness, therefore, no surface thermal exfoliation was observed by other authors.

Figure 2 a indicates the photocurrent–potential curves of the Ta_3N_5 samples at different oxidation temperatures, which shows that the photocurrent increases with increasing oxidation temperature of the Ta foils. However, the variation relationship between photocurrent and oxidation temperature is not linear (Figure 2 b). The photocurrent at 1.23 V versus RHE slowly enhances with the increase of oxidation temperature from 550 to 570 °C, then sharply increases from 570 to 590 °C, and then slowly increases to 610 °C. The results indicate that 570 °C is the critical knee point for the photocurrent enhancement. To understand the reason for nonlinear changes of the photocurrent, the average crystal grain size and relative electrochemical active area were calculated by the Scherrer equation and Jaramillo's method, respectively.[21] The results suggest that the grain sizes are very similar (Table S1a) and that the sample at 570 °C has the higher relative electrochemical surface area (Figure S3). For a Ta_3N_5 photoanode, the electrochemical surface area is higher, and the photocurrent is higher.[21] However, the photocurrent of the sample at 570 °C is much lower than that of the sample at 590 °C. Therefore, the photocurrent jumping from 570 to 590 °C does not result from better crystallinity or higher surface area, but from the exfoliation of the surface layer.

To further verify the effect of the surface layer on the photocurrent, we applied a facile mechanical exfoliation method to remove the surface layer of the Ta_3N_5 sample at 570 °C with scotch tape, which can completely exclude an effect of temperature. After mechanical exfoliation, the Ta_3N_5 sample at 570 °C exhibit a surface morphology (Figure 1 k) similar to the samples at 590 and 610 °C (Figure 1 c, Figure 1 d) after thermal exfoliation. The photocurrents of the Ta_3N_5 samples at 570 °C before and after mechanical exfoliation of the surface layer were investigated (Figure 2 c). The photocurrent of the sample at 570 °C after mechanical exfoliation increased to a similar value to that of the sample at 590 °C (Figure 2 b). We also used the same mechanical exfoliation method to remove the surface layer of the thinner Ta_3N_5 sample at 550 °C, but there was no obvious enhancement of the photocurrent because of the tight connection between the surface layer and the under part (Figure 1 j). Alternatively, we removed the surface layer by etching Ta_3N_5 in 40 % hydrofluoric acid solution for 1 minute. After HF treatment, a thin and smooth surface layer of Ta_3N_5 was removed, and the Ta_3N_5 particles were exposed (Figure S4). The photocurrent of Ta_3N_5 at 550 °C also increased after surface treatment by HF solution (shown in Figure S5). These results further confirm that the removal of the surface layer is the main reason for the photocurrent enhancement. The composition of the surface layer in different depths was

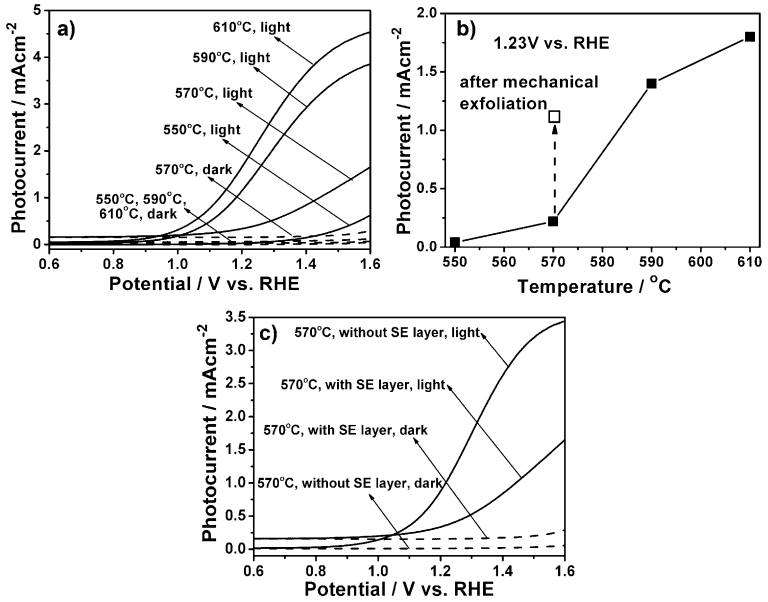

Figure 2. a) Photocurrent–potential curves of the Ta_3N_5/Ta electrodes at different oxidation temperatures (550–610 °C). b) The photocurrent of samples at different oxidation temperatures at 1.23 V versus RHE. c) Photocurrent–potential curves of the Ta_3N_5/Ta electrodes at 570 °C before and after mechanical exfoliation of the surface layer. Electrolyte: 1 M NaOH, light source: AM1.5G sunlight simulator (100 mW cm^{-2}).

investigated by X-ray photoelectron spectroscopy (XPS; Tables S2–S4 and Figures S6–S7). The results show that the surface exfoliation layer consists of a passivation layer (a thin layer of $Ta_{3-x}N_{5-y}O_y$ (<15 nm) with Ta vacancies and O impurities and a Ta_3N_5 layer. The composition details are described in Supporting Information.

We used electrochemical impedance spectroscopy (EIS) and photoluminescence spectroscopy to study the interface charge transfer and recombination process of the photogenerated carriers before and after the exfoliation of the surface passivation layer.[28,29] R_{ct}, the semiconductor–electrolyte charge-transfer resistance, is a key parameter in characterizing the semiconductor-electrolyte charge transfer process. We quantitatively simulated the R_{ct} values from the EIS spectra in Figure 3a and b and the results are shown in Figure S8. Under illumination, the R_{ct} of the sample sharply decreases after mechanical or thermal exfoliation. Generally, the larger the R_{ct} value, the slower is the interface charge transfer.[28,29] Therefore, the results suggest that the interface charge transfer of photogenerated carriers becomes much faster after surface exfoliation.

The slow interface charge transfer in the samples with the surface layer is further verified by photoluminescence spectra (Figure 3c). Two emission peaks at about 510 and 610 nm are observed in the samples. The photoluminescence intensity decreases obviously after thermal or mechanical exfoliation of the surface layer. To identify the emission peaks, photoluminescence spectra of commercial Ta_2O_5 and Ta_3N_5 powders prepared by nitridation of commercial Ta_2O_5 were also measured and the results are shown in Figure S9. Two similar emission peaks are also observed in the commercial Ta_2O_5 powders, whereas no peaks are observed for the Ta_3N_5 powders.[30] Therefore, the 510 nm and 610 nm peaks may stem from the amount of residual O^{2-} in the surface passivation layer, which form recombination centers of photogenerated carriers. The EIS and PL results suggest that the density of the surface recombination centers becomes less after removal of the surface passivation layer, which remarkably reduces recombination of photogenerated carriers and enhances the photocurrent. According to the above discussion, a schematic diagram of the photocurrent improvement mechanism after thermal or mechanical exfoliation is indicated in Figure 4. Recently, we also found that surface pretreatment had similar effects on the Mo-doped $BiVO_4$ and InGaN photoanodes.[31,32] Therefore, the removal of surface recombination centers can be a universal strategy to improve the photoelectrochemical performance of a photoelectrode.

In previous studies, $Co(OH)_x$ surface loading could significantly improve the photocurrent and photostability of Ta_3N_5 photoanodes.[20,33] Therefore, $Co(OH)_x$ was also used in this study to further improve the performance of the sample. Taking Ta_3N_5 at 570 °C, for example, after the

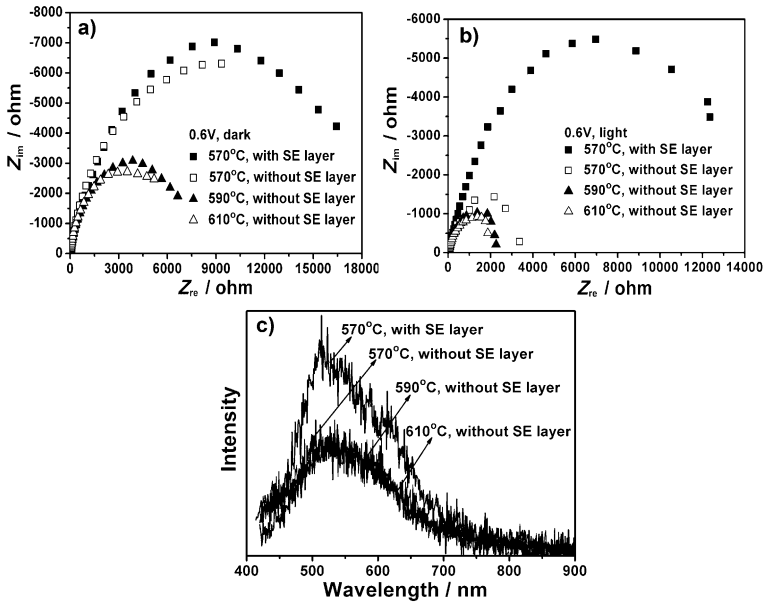

Figure 3. Electrochemical impedance spectroscopy and photoluminescence spectra of the Ta_3N_5/Ta electrodes at 570 °C (before and after mechanical exfoliation of the surface passivation layer), the sample at 590 °C and the sample at 610 °C (after thermal exfoliation). a) EIS in the dark. b) EIS under illumination. Potential: 1.6 V versus RHE, electrolyte: 1 M NaOH. c) Photoluminescence spectra with an excitation wavelength of 330 nm.

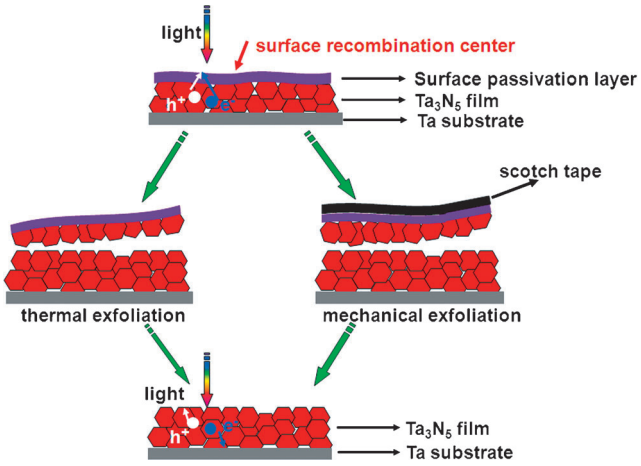

Figure 4. Mechanism of the photocurrent improvement after surface thermal and mechanical exfoliation.

surface mechanical exfoliation, the photocurrent onset potential of the sample shifts negatively and the saturated photocurrent increases about 100% after $Co(OH)_x$ loading (Figure 5a). However, without the surface mechanical exfoliation, only the photocurrent onset potential shifts negatively, the saturated photocurrent does not obviously increase after $Co(OH)_x$ loading. The results also suggest that the charge transfer of photogenerated carriers in the surface layer is a limit step.

The photocurrent–potential curves of the $Co(OH)_x$-loaded Ta_3N_5 samples at 550–610°C were measured and the results suggested that the sample at 610°C had the highest photocurrent (Figure S10). Figure 5b shows the photocurrent of the bare Ta_3N_5 and $Co(OH)_x$-loaded Ta_3N_5 at 610°C, the onset potential negatively shifts about 0.2 V and the saturated photocurrent increases about 85% after $Co(OH)_x$ loading. The photocurrent onset potential after $Co(OH)_x$ loading is about 0.82 V versus RHE, which is close to the values (about 0.85 V versus RHE) reported by us and others.[20,24] For a bare Ta_3N_5, photogenerated holes are accumulated on the surface of the electrode because of slow interface charge transfer, which leads to serious recombination and photocorrosion. After $Co(OH)_x$ is loaded on the photoelectrode as a water oxidation electrocatalyst, photo-generated holes in Ta_3N_5 can migrate to $Co(OH)_x$ more quickly, which suppresses the recombination and photocorrosion of the photoelectrode. The solar photocurrent at 1.23 V versus RHE is about 5.5 mA cm^{-2} from the photocurrent–potential curve. The photocurrent at 1.23 V versus RHE was also further confirmed by an photocurrent–time curve, which excludes the effect of capacitive current (Figure S11). The solar photocurrent was also calculated by integrating incident photon-to-current efficiencies (IPCEs) with the standard solar spectrum following Gratzel's method to exclude the difference between the simulated AM1.5G light source and the real solar spectrum.[16,17] The IPCE at 1.23 V versus RHE is about 50% at 400–470 nm (Figure 5c) and the photoresponse wavelength is about 600 nm, which is close to the absorption edge of Ta_3N_5. The integrated photocurrent (5.2 mA cm^{-2}, Figure S12) is very close to the measured value, which suggests that the measured solar photocurrent is reliable. In addition, we also measured solar photocurrent in aqueous solution at pH = 13 to compare with the value in ref. [24], a value of 5.2 mA cm^{-2} at 1.23 V versus RHE was obtained. The highest solar photocurrents at 1.23 V versus RHE for the Ta_3N_5 photoanode have been previously reported as about 3.8 mA cm^{-2}.[20,24] Therefore, we have obtained the highest solar photocurrent among all currently available Ta_3N_5 photoanodes. The solar energy conversion efficiency[5,34] of the $Co(OH)_x$-loaded Ta_3N_5 photoanode is calculated as 0.51% at 1.06 V versus RHE from Figure 5b (shown in Figure S14).

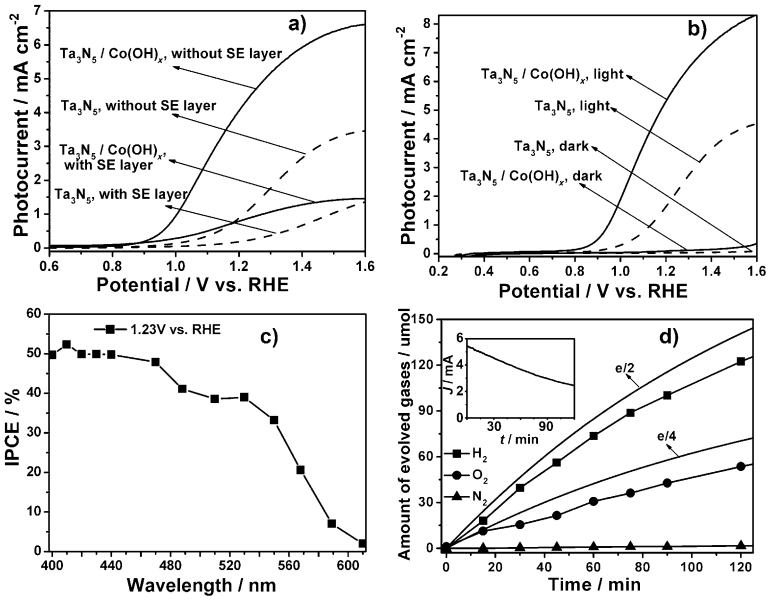

Figure 5. a) Photocurrent–potential curves of the samples at 570°C, with and without $Co(OH)_x$ loading, before and after surface exfoliation, 1 M NaOH, AM1.5G (100 mW cm^{-2}) illumination. The photocurrent here is the difference value between the photocurrent and the dark current. b) Measured AM1.5G (100 mW cm^{-2}) photocurrent–potential curves of bare Ta_3N_5/Ta and the $Co(OH)_x$-loaded Ta_3N_5/Ta electrodes at 610°C, 1 M NaOH, scan rate: 10 mV s^{-1}. c) IPCE at 1.23 V versus RHE of the Ta_3N_5/Ta electrodes at 610°C with $Co(OH)_x$ surface loading. The IPCE action spectrum was measured by steady-state photocurrent. d) Time courses of gas evolution from the $Co(OH)_x$-loaded Ta_3N_5 at 610°C in a two-electrode cell under AM1.5G (100 mW cm^{-2}) illumination, 1 M NaOH, the bias was 1.23 V. The area of the Ta_3N_5 was about 1 cm^2. The inset shows the photocurrent–time curve under illumination.

Moreover, stability and Faradaic efficiency for a non-oxide photoanode are especially important. They were measured and the results are indicated in Figure 5d. The photocurrent of a $Co(OH)_x$-loaded Ta_3N_5 photoanode at 610°C decreases about 55% after 2 h of illumination. The photostability of a photoelectrode depends on the light intensity. A higher light intensity leads to a reduced stability.[35] H_2 and O_2 bubbles were observed on the Pt cathode and the Ta_3N_5 photo-

anode, respectively (Figure S15). The Faradaic efficiencies of H_2 and O_2 are about 85 and 74%, respectively. The Faradaic efficiency of O_2 is 11% less than that of H_2 because some Ta_3N_5 is oxidized by photogenerated holes. N_2 was released during the Faradaic efficiency measurement, which suggested that Ta_3N_5 was partially photocorroded. This result is also verified by XPS measurements of Ta_3N_5 before and after the Faradaic efficiency test (Figure S16). We have compared the photostability and Faradaic efficiencies of the $Co(OH)_x$-loaded Ta_3N_5 samples at 570°C (before the surface exfoliation) and 610°C (after the surface exfoliation) under illumination with the same light intensity, and observed that photostability and Faradaic efficiencies are similar for both samples (Figure 5d and Figure S17). The results exclude the possibility that the increase in the photocurrent by removing the surface layer stems from the enhanced photocorrosion of the Ta_3N_5 electrode.

In summary, the photocurrent of Ta_3N_5 was improved remarkably by thermal or mechanical exfoliation of the surface recombination centers. This strategy can offer guidance to improve photoelectrochemical performance of other materials. After further modification of the electrocatalyst on Ta_3N_5, we obtained a solar photocurrent of 5.5 mA cm^{-2} at 1.23 V versus RHE, which is the highest value among all currently available Ta_3N_5 photoanodes. Future work will be carried out to shift the photocurrent onset potential negatively and improve the photostability of this material for practical applications.

Received: June 21, 2013
Revised: July 30, 2013
Published online: August 14, 2013

Keywords: electrochemistry · hydrogen production · photochemistry · surface chemistry · water splitting

[1] G. W. Crabtree, M. S. Dresselhaus, M. V. Buchanan, *Phys. Today* **2004**, *57*, 39 – 44.
[2] A. Fujishima, K. Honda, *Nature* **1972**, *238*, 37 – 38.
[3] A. B. Murphy, P. R. F. Barnes, L. K. Randeniya, I. C. Plumb, I. E. Grey, M. D. Horne, J. A. Glasscock, *Int. J. Hydrogen Energy* **2006**, *31*, 1999 – 2017.
[4] W. Shockley, H. J. Queisser, *J. Appl. Phys.* **1961**, *32*, 510 – 519.
[5] M. G. Walter, E. L. Warren, J. R. McKone, S. W. Boettcher, Q. Mi, E. A. Santori, N. S. Lewis, *Chem. Rev.* **2010**, *110*, 6446 – 6473.
[6] A. J. Nozik, *Appl. Phys. Lett.* **1976**, *29*, 150 – 153.
[7] Y. Hou, B. L. Abrams, P. C. K. Vesborg, M. E. Björketun, K. Herbst, L. Bech, A. M. Setti, C. D. Damsgaard, T. Pedersen, O. Hansen, J. Rossmeisl, S. Dahl, J. K. Nørskov, I. Chorkendorff, *Nat. Mater.* **2011**, *10*, 434 – 438.
[8] S. W. Boettcher, E. L. Warren, M. C. Putnam, E. A. Santori, D. Tuner-Evans, M. D. Kelzenberg, M. G. Walter, J. R. McKone, B. S. Brunschwig, H. A. Atwater, N. S. Lewis, *J. Am. Chem. Soc.* **2011**, *133*, 1216 – 1219.
[9] B. Seger, A. B. Laursen, P. C. K. Vesborg, T. Pedersen, O. Hansen, S. Dahl, I. Chorkendoff, *Angew. Chem.* **2012**, *124*, 9262 – 9265; *Angew. Chem. Int. Ed.* **2012**, *51*, 9128 – 9131.
[10] M. H. Lee, K. Takei, J. Zhang, R. Kapadia, M. Zheng, Y. Chen, J. Nah, T. S. Matthews, Y. Chueh, J. W. Ager, A. Javey, *Angew. Chem.* **2012**, *124*, 10918 – 10922; *Angew. Chem. Int. Ed.* **2012**, *51*, 10760 – 10764.
[11] B. D. Alexander, P. J. Kulesza, I. Rutkowska, R. Solarska, J. Augustynski, *J. Mater. Chem.* **2008**, *18*, 2298 – 2303.
[12] N. Gaillard, B. Cole, J. Kaneshiro, E. L. Miller, B. Marsen, L. Weinhardt, M. Bär, C. Heske, K.-S. Ahn, Y. Yan, M. M. Al-Jassim, *J. Mater. Res.* **2010**, *25*, 45 – 51.
[13] W. Luo, Z. Yang, Z. Li, J. Zhang, J. Liu, Z. Zhao, Z. Wang, S. Yan, T. Yu, Z. Zou, *Energy Environ. Sci.* **2011**, *4*, 4046 – 4051.
[14] Y. Park, K. J. McDonald, K. S. Choi, *Chem. Soc. Rev.* **2013**, *42*, 2321 – 2337.
[15] Z. S. Li, W. J. Luo, M. L. Zhang, J. Y. Feng, Z. G. Zou, *Energy Environ. Sci.* **2013**, *6*, 347 – 370.
[16] S. D. Tilley, M. Cornuz, K. Sivula, M. Grätzel, *Angew. Chem.* **2010**, *122*, 6549 – 6552; *Angew. Chem. Int. Ed.* **2010**, *49*, 6405 – 6408.
[17] K. Sivula, F. L. Formal, M. Grätzel, *ChemSusChem* **2011**, *4*, 432 – 449.
[18] A. Ishikawa, T. Takata, J. N. Kondo, M. Hara, K. Domen, *J. Phys. Chem. B* **2004**, *108*, 11049 – 11053.
[19] M. Higashi, K. Domen, R. Abe, *Energy Environ. Sci.* **2011**, *4*, 4138 – 4147.
[20] M. Liao, J. Feng, W. Luo, Z. Wang, J. Zhang, Z. Li, T. Yu, Z. Zou, *Adv. Funct. Mater.* **2012**, *22*, 3066 – 3074.
[21] B. A. Pinaud, P. C. K. Vesborg, T. F. Jaramillo, *J. Phys. Chem. C* **2012**, *116*, 15918 – 15924.
[22] Y. Cong, H. S. Park, H. X. Dang, F. F. Fan, A. J. Bard, C. B. Mullins, *Chem. Mater.* **2012**, *24*, 579 – 586.
[23] Y. Cong, H. S. Park, S. Wang, H. X. Dang, F.-R. F. Fan, C. B. Mullins, A. J. Bard, *J. Phys. Chem. C* **2012**, *116*, 14541 – 14550.
[24] Y. Li, T. Takata, D. Cha, K. Takanabe, T. Minegishi, J. Kubota, K. Domen, *Adv. Mater.* **2013**, *25*, 125 – 131.
[25] Y. Lin, Y. Xu, M. T. Mayer, Z. I. Simpson, G. McMahon, S. Zhou, D. Wang, *J. Am. Chem. Soc.* **2012**, *134*, 5508 – 5511.
[26] S. J. Moon, W. W. So, H.-Y. Chang, *J. Electrochem. Soc.* **2001**, *148*, E378 – E381.
[27] Y. Jin, J. Y. Song, S.-H. Jeong, J. W. Kim, T. G. Lee, J. H. Kim, J. Hahn, *J. Mater. Res.* **2010**, *25*, 1080 – 1086.
[28] F. Le Formal, N. Tétreault, M. Cornuz, T. Moehl, M. Grätzel, K. Sivula, *Chem. Sci.* **2011**, *2*, 737 – 743.
[29] B. Klahr, S. Gimenez, F. Fabregat-Santiago, T. Hamann, J. Bisquert, *J. Am. Chem. Soc.* **2012**, *134*, 4294 – 4302.
[30] H. Shin, S. Y. Park, S. T. Bae, S. Lee, K. S. Hong, H. S. Jung, *J. Appl. Phys.* **2008**, *104*, 116108.
[31] M. Li, W. Luo, B. Liu, X. Zhao, Z. Li, D. Chen, T. Yu, Z. Xie, R. Zhang, Z. Zou, *Appl. Phys. Lett.* **2011**, *99*, 112108.
[32] W. J. Luo, Z. S. Li, T. Yu, Z. G. Zou, *J. Phys. Chem. C* **2012**, *116*, 5076 – 5081.
[33] C. Zhen, L. Wang, G. Liu, G. Q. Lu, H. Cheng, *Chem. Commun.* **2013**, *49*, 3019 – 3021.
[34] R. Saito, Y. Miseki, K. Sayama, *Chem. Commun.* **2012**, *48*, 3833.
[35] J. A. Seabold, K. Choi, *J. Am. Chem. Soc.* **2012**, *134*, 2186.

